Idrisov, R.; Floris, I.; Rothhardt, M.; Bartelt, H. (2021). Characterization and calibration of shape sensors based on multicore optical fibre. Optical Fiber Technology. 61:1-8. https://doi.org/10.1016/j.yofte.2020.102319

Characterization and calibration of shape sensors based on multicore optical fibre

Ravil Idrisov[a], Ignazio Floris[b,c], Manfred Rothhardt[a], Hartmut Bartelt[a]

[a]*Leibniz Institute of Photonic Technology, Albert-Einstein-Straße 9, Jena, 07745, Germany*
[b]*ITEAM , Universitat Politècnica de València, Camino de Vera s/n, Valencia, 46022, Spain*
[c]*ICITECH, Universitat Politècnica de València, Camino de Vera s/n, Valencia, 46022, Spain*

Abstract

In order to provide high accuracy in shape measurement with multicore optical fibres, characterization and calibration procedures are an important part of sensor preparation. Some procedures can be considered mandatory for adequate shape reconstruction, while others can help to enhance the measurement accuracy. Several of such procedures are discussed and experimentally applied for demonstrating the possible performance enhancement of curvature sensing, a fundamental phase of the shape reconstruction process. The maximum error observed in curvature calculation for a test object has been proved to be almost halved, decreasing from 2.48% to 1.36%, by applying such calibration corrections. The overall average relative accuracy of curvature measurement was improved from 0.89% to 0.5% (an improvement of 44%).

Keywords: *Shape sensor, Curvature sensor, Fiber Bragg grating, Multicore fiber, Sensor calibration, Optical fiber sensor*

1. INTRODUCTION

Over the past 10 years there has been an increasing interest in shape sensors based on optical fibres for various applications. Since 2000, when the first bent sensor based on multicore fibre was reported [1], extensive research efforts have been focused on the development of shape sensors using multicore fibres and fibre bundles and exploiting Rayleigh [2] and Brillouin [3] scattering and fibre Bragg gratings (FBGs) [4]. These technologies use different interrogation principles to measure strain along the length of an optical fibre. While we discuss in this work a series of calibration procedures for the case of shape sensors based on FBG reflection peak tracking, similar concepts may be also applied to sensors based on other sensing technologies.
Because of their good spatial resolution and high measurement frequency rate, fibre-grating-based shape sensors have especially been investigated for implementation in medical needles, endoscopes and robotic systems [5]. Shape measurement is based on the interpretation of the strain along the fibre as a combination of curvature, twist and longitudinal strain. In general, the methods for shape reconstruction calculate the shape from local variations of curvature. In the case of medical applications, of great importance is not only the general object shape, but also the tracking of the sensor tip coordinates, which is sensible to the accumulated shape measurement error along the full sensor length. The reduction of these errors, based on applying different interpolation techniques for shape reconstruction using quasi-distributed sensors has been shown in the literature [6]. In this paper, in order to limit error propagation, we examine a series of factors, including sensor geometry, photo-elastic coefficient, Bragg wavelength reference and presence of twist, that influence the accuracy in curvature sensing, a fundamental stage in the shape reconstruction process. Moreover, we present a methodology for shape sensor calibration and characterization and discuss the results of an experimental study performed to validate it, considering shape sensors constituted of multicore fibres with FBGs inscribed by an interferometric technique [7].

2. SHAPE SENSING CONCEPT

Optical shape sensing with FBGs in multicore optical fibres relies on the measurement of the strain distribution across the fibre cross-sections, caused by a combination of elongation or compression, bend and torsion (Fig. 1). The approaches to shape reconstruction determine the curvature along the sensor on the basis of strain measurements and calculate the shape through curvature interpolation and integration. One of the most widely used methods consists in the numerical integration of the Frenet-Serret equations, once the curvature and torsion function have been computed along the fibre length [8].

* Corresponding author.
E-mail address: ravil.idrisov@leibniz-ipht.de

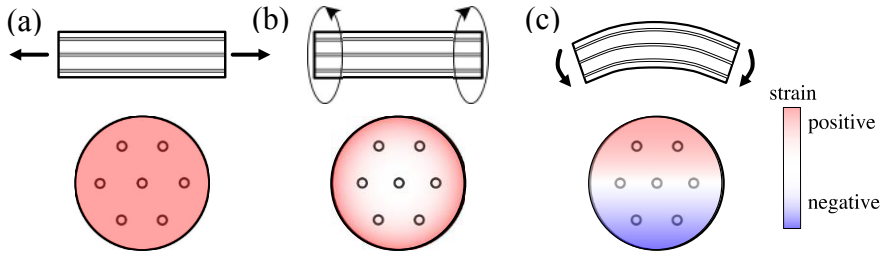

Fig.1. Strain distribution in stretched (a), twisted (b) and bent (c) multicore optical fibre.

The strain distribution along a multicore fibre depends on the type of deformation that each cross-section is subjected to. Stretching generates a uniform increase in strain throughout the cross-section of the fibre. Torsion has no effect on the centre of the fibre and reaches maximum strain on the fibre edges; therefore, only outer cores are experiencing strain. Bending introduces a gradient of strain over the cross-section with no strain on the neutral axis, perpendicular to the bend direction (Fig. 2). Reconstructing this gradient of strain in a multicore fibre and discriminating it from other types of deformation, using information from a combination of measurement points, is the main task of curvature and direction measurement along a sensing fibre. The combination of reconstructed curvature values and curvature direction parameters, then, allows performing a general shape measurement.

The local curvature κ of a bent multicore fibre, defined as the inverse local bending radius, R, can be described mathematically at a certain position along the fibre as [8]:

$$\kappa = \frac{\sqrt[2]{(\sum_{i=1}^{N} \frac{\varepsilon_i}{r_i} cos\theta_i)^2 + (\sum_{i=1}^{N} \frac{\varepsilon_i}{r_i} sin\theta_i)^2}}{N} \quad (1)$$

Here, ε_i and r_i are the curvature-caused strains measured in the single core i and the distance from the core i to the centre of the fibre, N is the number of cores used for curvature calculation; θ_i is the angle between one of the axes of the coordinate system, which can be associated with core 1 relative to core i (Fig. 2). For each grating of the longitudinal array, the curvature is an averaged value, calculated by using the measured strain of N cores in the transversal FBG array. Therefore, the correct and efficient strain measurement in each core affects the overall curvature calculation.

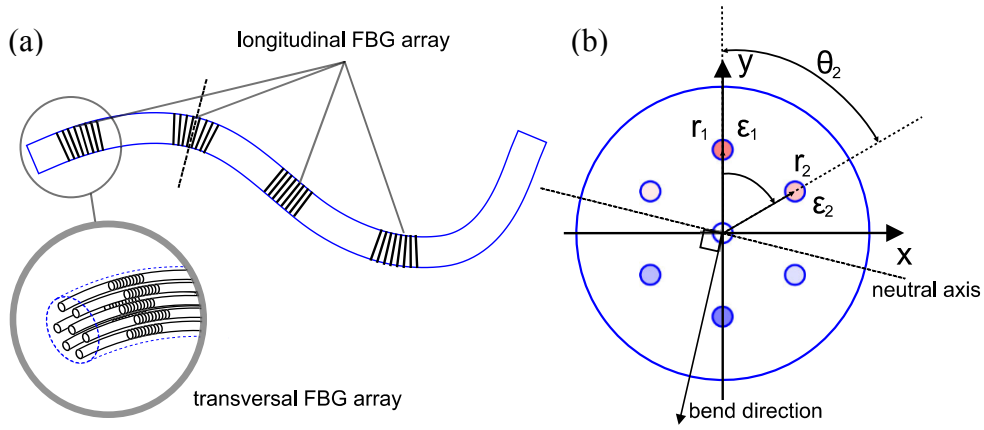

Fig. 2. Schematic of a bent multicore fibre (a) with core orientations and radial distances and strains indicated for two cores (b).

With the calculated curvature, then, the local neutral axis and an angular distance to the neutral axis can be defined for each core. We can then calculate the bending angle between the neutral axis and the coordinate system associated with one of the cores, using strain information in the core nearest to the neutral axis:

$$\theta_{bend} = \arcsin\left(\frac{\varepsilon_i}{r_i \kappa}\right) - \theta_i \quad (2)$$

Knowledge about the local curvatures and the bending orientation then allows reconstruction of the continuous shape along the fibre by means of interpolation methods.

Shape measurement using arrays of FBGs as a quasi-distributed sensor requires knowledge about several parameters. Strain measurement based on FBGs is a method of measuring a fibre core elongation via a shift of the reflection peak wavelength for an inscribed FBG. For each core i, there is a relation between the local strain ε and the measurable wavelength shift $\Delta\lambda_B$ of the FBG reflection peak:

$$\varepsilon = \frac{\lambda_m - \lambda_B}{\lambda_B(1-p_e)} \tag{3}$$

with λ_B and λ_m being the initial and the measured strained wavelength peak position, respectively, and p_e being the photo-elastic coefficient that has to be measured once for a specific fibre. Local strain, ε, is generally defined by a relative elongation $\varepsilon = \Delta L/L$.

Therefore, for reconstructing a certain curvature, the wavelengths of Bragg reflection peaks λ_m for each grating have to be measured and a number of other parameters such as θ_i, r_i, λ_B, p_e have to be known from characterization or calibration measurements. Some of these parameters can be measured directly, others are derived indirectly by a calibration procedure. In the following sections we will separately discuss the procedures for determining these parameters, and we will show the improvements in curvature measurement accuracy for a test object. Due to the fact that the general curvature reconstruction is based on differential measurements, the exact knowledge of these parameters is of great interest, in order to limit possible error accumulation along the length of the fibre sensor.

2.1. Fibre geometry

A number of multicore fibres has been reported in the literature [9] for application in shape sensing. The use of each particular fibre for shape sensing requires knowledge about its geometry – such as the number of cores N, the core-to-centre distance r_i, and the angle θ_i. This information can be obtained from a microscope cross section image (Fig. 3). For our investigations we used a seven-core fibre as shown in Fig. 2. The geometrical parameters shown were derived from a microscopic image of such a fibre cross-section.

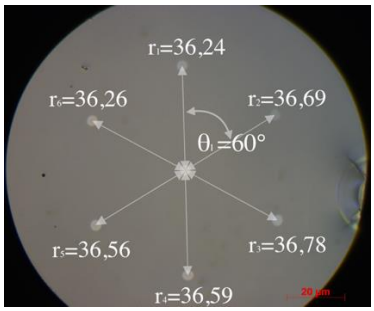

Fig. 3. Microscope image of an experimental 7-core fibre, with geometrical parameters.

Besides the specific values of the core-to-centre distances (also called core spacing), the knowledge of the relative variations (the ratio of the core distance relative to the average distance) would be an important parameter for the reconstruction algorithm. In our case, the core-to-centre distances for the position shown are in a range of 36.24-36.78 µm. Due to the small variation, usually one single averaged value of the core-to-centre distance is used for the reconstruction algorithm to avoid associating each core with a specific value. The effect of such averaging has been discussed in the literature [10]. However, a variation of such core-to-centre distances may occur along the fibre as discussed in section 2.2.

2.2. Photo-elastic coefficient

The photo-elastic coefficient (p_e) describes the strength of the change of optical properties of the material under mechanical deformation. As applied to an optical fibre, this parameter defines the change of the effective refractive index in response to physical fibre deformation. For such a case, a single characterization or calibration measurement of a single measured photo-elastic coefficient p_m (e.g. in the central core) would be sufficient to determine this parameter. It has to be considered, however, that the multicore fibre manufacturing process might introduce individual modifications of the different fibre cores as well as variations of the structural parameters, e.g. fibre and core diameters or material/doping distributions. Such variations can be considered as an additional

correction factor α_i, measured experimentally during a calibration procedure, which would have to be included in the curvature calculation algorithm (4). In case of strain gauges based on FBGs, this coefficient also defines the shift of the reflection peak wavelength.

$$\Delta\lambda_B = \lambda_B(1 - p_m\alpha_i)\varepsilon \tag{4}$$

A setup that can stretch the fibre and associate the elongation with the peak wavelength shift is shown in Fig. 4.

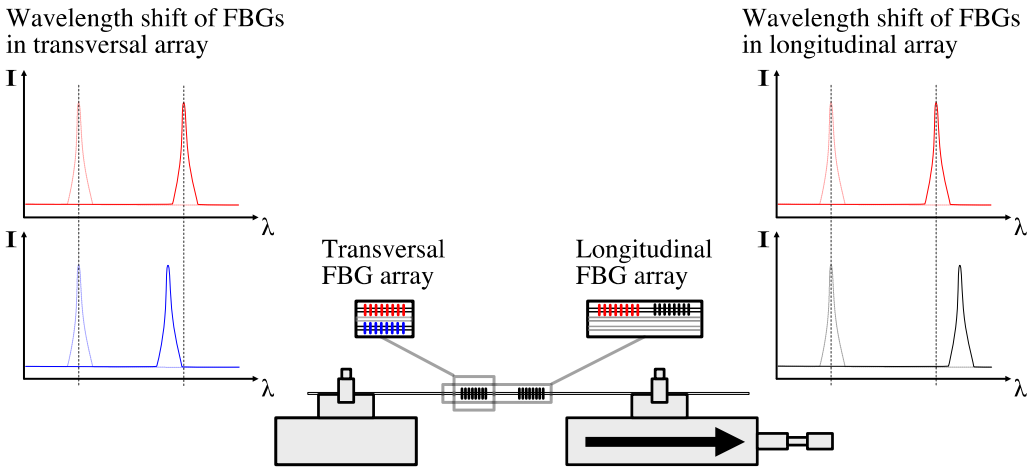

Fig. 4. Setup for photo-elastic (p_e) and correction coefficient (α_i) measurement.

Photo-elastic coefficient measurement and correction coefficients α_i are crucial for converting the measured wavelength shift data into strain, which is later used for curvature calculation. In order to measure the variation of the photo-elastic coefficients in different cores and along the fibre, the fibre was stretched to track the wavelength shift of the FBG in the array in the central and three outer cores of the fibre. The measured wavelength shifts in the cores are shown in Fig. 5.

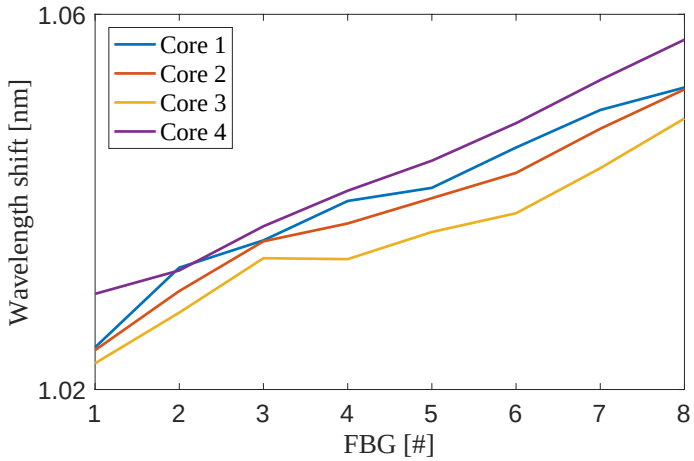

Fig. 5. Wavelength shift in an array of FBGs in the stretched fibre.

As can be seen from Fig. 5, the peak wavelength shift differs in the cores of the fibre for 9 pm on average. This will define α_i coefficients in the range of 0.9819-1.0054. Moreover, the shift is growing over the sensor length for each core by about 27 pm. This means that the stretched fibre has non-uniform strain along the sensing length due to varying fibre diameter, which can be measured and compensated via correction factors γ_j (0.9913-1.0125), interpreted as a change of the fibre diameter for each FBG of the longitudinal array and, hence, the core-to-centre distance r_i. The final equation by which we calculate the curvature in the *j-th* grating, using the strain measured in N cores and considering the correction factors, is

$$\kappa_j = \frac{\sqrt[2]{\left(\sum_{i=1}^{N}\frac{\varepsilon_{i,j}}{r_i\gamma_j}cos\theta_i\right)^2+\left(\sum_{i=1}^{N}\frac{\varepsilon_{i,j}}{r_i\gamma_j}sin\theta_i\right)^2}}{N} \tag{5}$$

2.3. Initial fibre Bragg gratings reflection peak wavelengths

For the measurement of wavelength shifts, the knowledge of the exact starting conditions is mandatory. The spectra shown in Fig. 6 were measured for gratings simultaneously recorded by a single laser pulse in seven cores of a multicore fibre.

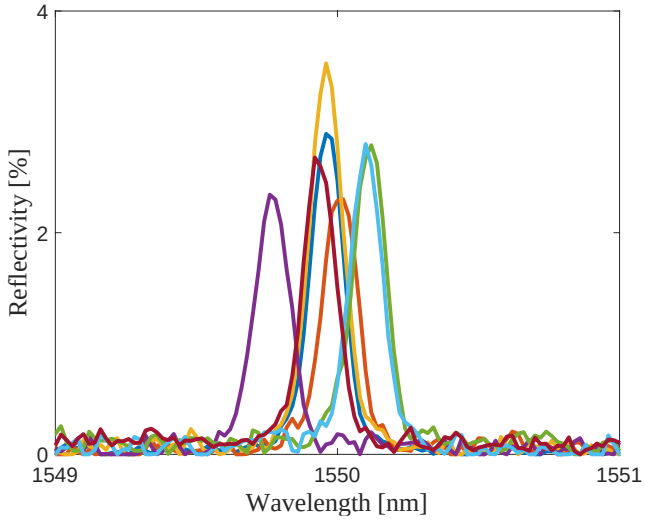

Fig. 6. Spectra of FBGs recorded in seven cores of a multicore fibre.

There are obvious differences in peak position and reflection peak strength. The wavelength in this case varies between 1549.77 and 1550.12 nm, and the reflectivity varies between 2.3 and 3.5%. These variations can be attributed to differences in the effective refractive index of different cores and to variations of the grating modulation depth due to lensing and shadowing effects produced during the inscription of gratings in a multicore optical fibre.
Therefore, the initial reflection peak wavelength of the gratings in all cores has to be identified. In general, such measurements are a standard procedure. For high-accuracy measurements, it should be considered that such measurements would be temperature-sensitive and that any additional strain due to bend, twist or axial load during the characterization procedure should be avoided. Clamping optical fibres on both sides can cause twist and bend in the fibre. It is also difficult to set the fibre in a straight condition horizontally without strong stretching due to the gravity effect on the fibre. Therefore, a setup with the fibre clamped on one side is favourable. (Fig. 7). The fibre is suspended vertically in this case and, to straighten the fibre, a load of few grams can be fixed at the end of the fibre. This load leads to a wavelength shift of the reflection peaks from the initial position. However, the effect of the negative strain measured by the system can be considered and corrected later in the processing of the measurement data.

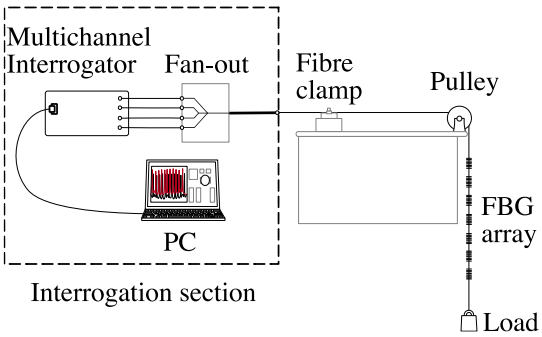

Fig. 7. Setup for initial FBG reflection peak wavelength measurement.

This method allows the fibre to take its natural shape and prevents any additional torsion and curvature.

2.4. Intrinsic twist measurement

The manufacturing and handling process can cause a twist along an optical fibre, which results in a helically twisted positioning of the fibre cores. In a shape measurement procedure, this twist cannot be discriminated from experimentally measured twist. Hence, a fibre curved in a plane would then seem to have a helical shape in the

reconstruction of the shape measurement. Since it is hard to control or reduce this twist, the shape sensor fibre has to be calibrated to reduce a shape error due to an intrinsic twist. It may also happen that a fibre is intentionally twisted during the manufacturing process. Also, in this case, the twist has to be well characterized.
For the intrinsic twist characterization, two different procedures are presented here. With the first method, the inner structure of the fibre is observed in a diffraction projection pattern from a side-illuminated fibre. Applying this procedure requires installing the fibre without adding an additional twist by handling the fibre. This can be achieved by hanging the loaded fibre vertically clamped on top and then, after taking its natural shape, clamping the fibre end at the bottom. Then the fibre can be used for observation of its diffraction pattern through one complete rotation (Fig. 8a) and by scanning along its longitudinal axis (Fig. 8b).

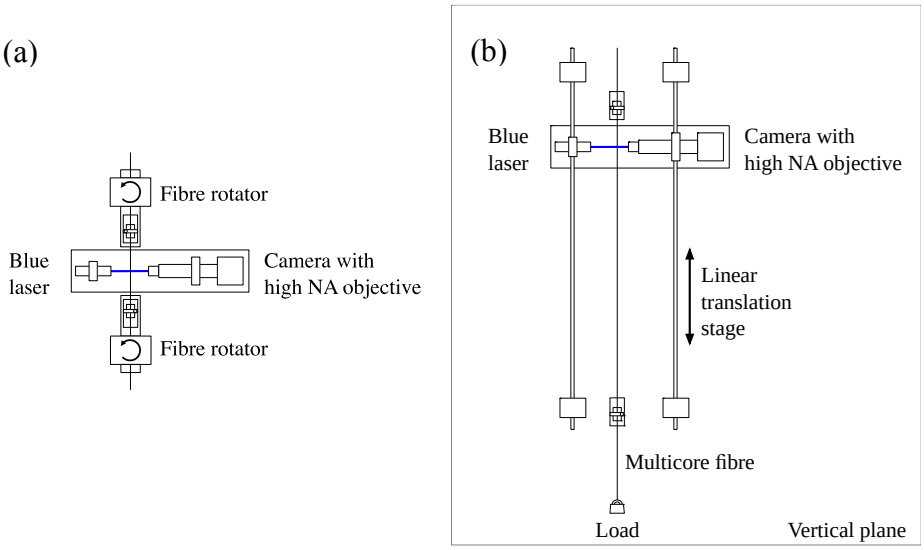

Fig. 8. Setups for intrinsic twist measurement using side laser illumination for fibre rotation (a) and fibre scanning (b).

In this setup, plane wave laser light is passing through the fibre and is diffracted and focused by the refractive and diffractive core structures. This light pattern is collected by an objective with high numerical aperture and projected into a camera. Dark areas in such recorded patterns correspond to the fibre cores. The position with the current angular orientation of the fibre becomes therefore detectable. Moving the illumination laser and the camera along the fibre enables recording the diffraction pattern for the given piece of the sensor (Fig. 9a) and comparing it with the pattern recorded for a complete rotation (Fig. 9b).

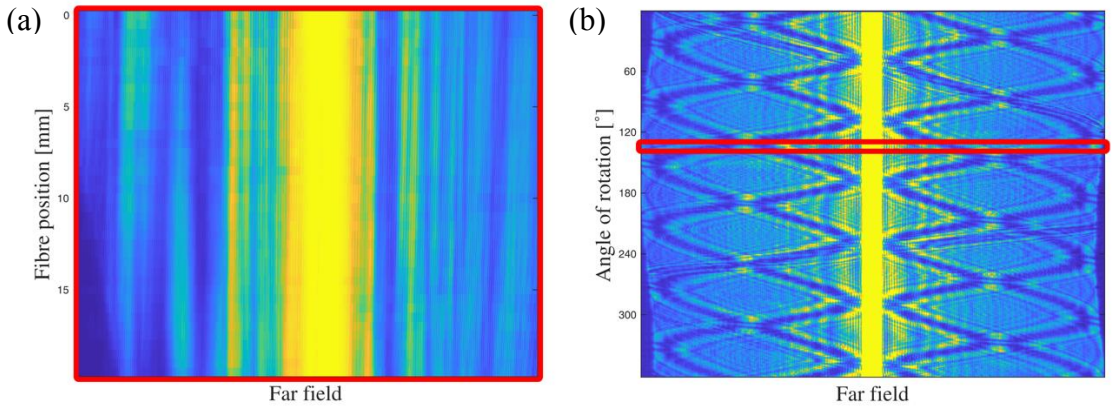

Fig. 9. Pattern formed by a stack of images obtained by scanning a length of 20 mm (a) and by one complete rotation of the 7-core fibre (b)

An analysis of these patterns allows quantification of the rotation angle of the cores in the given sensor length, which corresponds to the intrinsic twist of the fibre. The scanned pattern of 20 mm of fibre in our case shows the same pattern as a multicore fibre rotation from 131-134°, which corresponds to the twist of 1.5-2°/cm. This method does not require Bragg gratings to be inscribed in the cores and can be applied before FBG inscription. In this particular case, the measurement accuracy does not exceed 1-2°, since extracting the angle from the diffraction

pattern is limited due to the small variations along the scanning length applied. The accuracy of this method can be improved by a measurement of the distance between some distinct pattern structures that are formed in specific orientations and appear in a short range of rotation (<1°). Such distinct pattern structures can be observed with a periodicity corresponding to the fibre symmetry (60° in our case). Therefore, observing such distinct pattern structures twice during the fibre scanning can reveal an internal fibre torsion of 60° between the points where the patterns were detected. Since an angle of 60° is a rather large value of twist for a fibre, scanning of longer pieces of fibre might be necessary in this case: higher twist values are better to investigate and more easily detectable. Such a measurement can be achieved especially with a fibre with a designed twist of e.g. 50 rpm, since the shorter twist period in this case allows the scanning length to be reduced and the twist period to be measured with submillimetre accuracy.

The second method for twist measurement can be based on the shape measurement procedure of a known flat test shape structure applied with the same interrogation scheme as the one used for the general shape measurement. In this specific case, the measurement fibre is positioned in a curved shape on a flat plane surface (Fig. 10a). The bending radius must be small enough to ensure that the wavelength shift of the reflection peaks of FBGs in the cores caused by bend is larger than the possible noise level accuracy of the spectral measurement system. An intrinsic twist of the fibre will result in a reconstructed helical shape in the reconstructed fibre position beyond the real plane surface in the test setup (Fig. 10b), since, due to twist, a non-null value torsion will be detected [8].

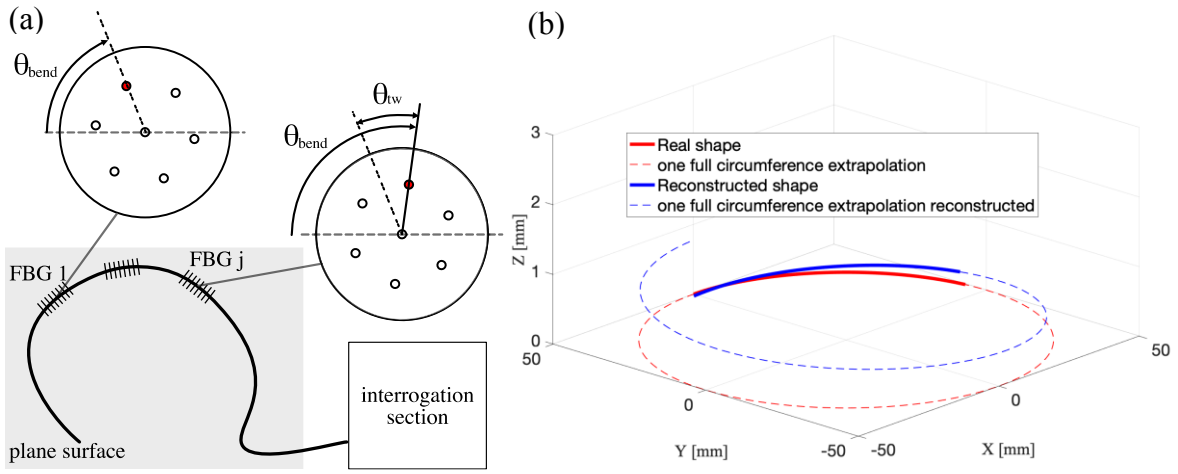

Fig. 10. Setup for the intrinsic twist measurement (a), shape reconstruction and real shape comparison for a twisted fibre (b).

The intrinsic twist is the measured change of the angle between the neutral axis and one of the cores for two different gratings of the longitudinal array. In our case, we performed the measurement several times to ensure measurement repeatability, and achieved an average intrinsic twist of 12.3° on the length of 72 mm between the centres of the first and the last gratings, which corresponds to the intrinsic twist of 1.71°/cm. This value will be used to correct the shape measurement for the intrinsic twist as a rotation of the coordinate system and will be subtracted from the bending angles measured.

The second intrinsic twist measurement method is simple and does not require additional equipment. It can be applied using the same interrogation system as that used for the shape measurement. The accuracy of the twist measurement achieves an accuracy below 1° and therefore better fits multicore fibres with a low intrinsic twist. Using a combination of the second method for the twisted fibre and the first method allows, in addition, an accurate measurement of the spacing between gratings, since in this case the FBG positions are associated with their angular orientation.

3. VALIDATION OF CALIBRATION CORRECTIONS WITH A TEST OBJECT

The impact of the discussed calibration corrections will now be shown for curvature measurements with a test object. A multicore fibre with 8 FBGs in each core and with a total length of 72 mm was used for the impact of the calibration procedures on the measurement accuracy. For defining a specific shape, we used a plane mould that has a set of grooves with different diameters representing shapes of different curvature. The sensing fibre was installed in the grooves with a defined curvature without clamping or gluing (Fig. 11).

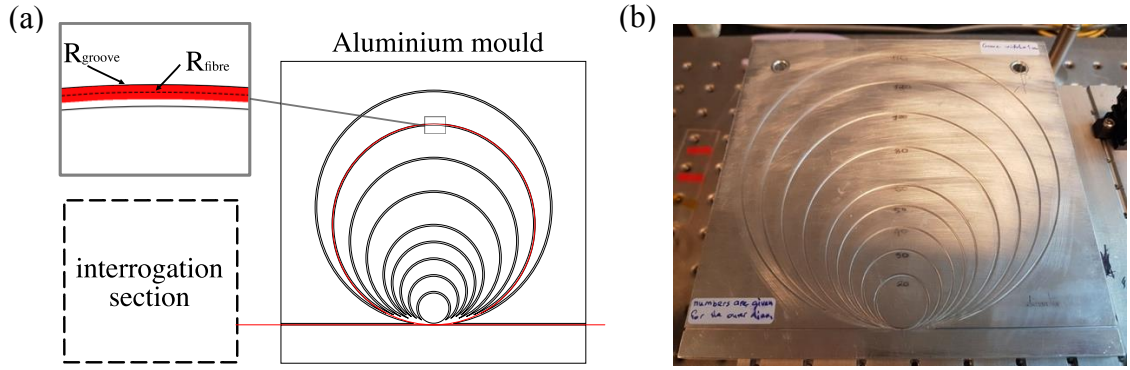

Fig. 11. Setup for positioning a sensing fibre in a plane test shape with fixed radii of curvature and a photograph of the aluminium mould.

The fibre was positioned in this plane mould with curvature radii R_{groove} of 40, 50, 60 and 70 mm so that all grating positions would experience the same bending with a radius, R_{fibre}, that is smaller than the radius of the groove, R_{groove}, for half the diameter of the fibre. Then the curvature can be calculated using equation (1), (Fig. 12a).

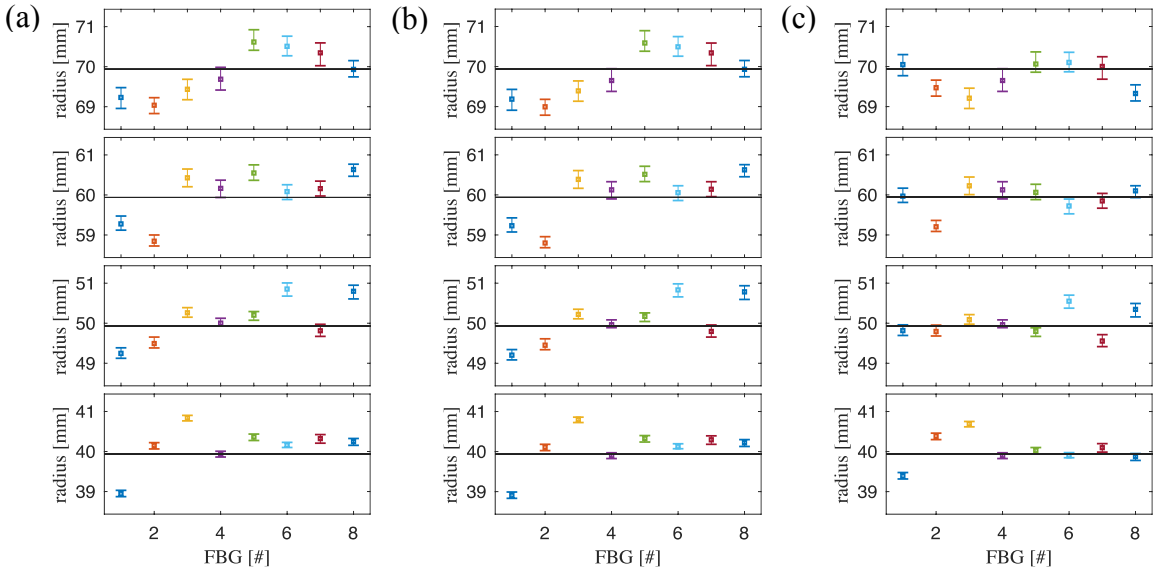

Fig. 12. Shape measurement of the grooves on the mould with no correction (a), with α (b) and additional γ (c) correction factors applied

Fig. 12a shows the reconstructed radii of curvature for 8 grating positions along the fibre length without use of the correction factors from calibration. Here, rectangles correspond to the averaged value of the radius of curvature as measured during the experiment. The bars indicate the range variation of 360 single measurements acquired with a frequency of 2 Hz. The theoretical curvature of the centre of the fibre, R_{fibre}, is shown as a black horizontal line. It is interesting to note that the variations in the single measurements are higher for larger curvature radii. The reason is that the reflection peak wavelength measurement error is affecting the fibre more strongly when it is bent with a larger radius, as it is subjected to lower strain and shows a lower peak wavelength shift in the cores. As a next step (Fig. 12b) the correction factors α were applied. In this case, the averaged relative error for all experiments slightly decreased from 0.89% to 0.88% (Fig. 12b). This minor change of accuracy indicates that the variation of the photo-elastic coefficient along the fibre is not high in our case and does not induce large additional errors for the curvature measurement.
For the results in Fig 12c, the correction factors of γ were applied in addition. In this case, the averaged error for the experiments performed decreased to 0.5%. For FBG #1, which showed the largest errors, the maximum observed error was almost halved, decreasing from 2.48% to 1.37%. This improvement indicates that the fibre diameter in our case varies along the fibre length in a range of 35.9-36.8 µm.

The calibration procedure enabled us to remarkably increase the accuracy in curvature sensing and to specify the calibration factors that individually tune the sensitivities of the longitudinal gratings array. The measurement of the photo-elastic coefficients (as material parameters) for the individual cores has a rather low impact on accuracy in our case because of low differences, but this procedure still should be applied in general, since photo-elastic coefficient differences are hard to predict for complex fibres. Using multicore fibres with a designed twist leads

to different wavelength shift-to-strain conversion factors for the helically twisted side cores and the straight central core; the α factor also can be used to take the conversion differences into account. The same calibration procedure is applied to check for local fibre diameter variations. In this way, one can identify fibre imperfections that are hard to check otherwise, and which have been shown to have a strong impact on the reconstruction accuracy. The calibration of the correction factors α and γ can be implemented with setups very similar to those for the initial reflection peak wavelengths measurement, by means of measuring the wavelength shifts of reflection peaks in each individual FBG in the longitudinal and transversal arrays.
The observed twist of 12.3° measured along a length of 17 cm is rather a high value for a fibre with no designed twist. This intrinsic twist information is important for the overall accuracy of the sensor when reconstructing a full 3D shape by combination of curvature magnitude and curvature direction data.

4. CONCLUSIONS

Calibration procedures for shape sensing with multicore optical fibres and inscribed FBGs have been shown and discussed. These procedures allow considering the sensitivity of each FBG in the array of the cores by elaborating the effective photo-elastic coefficient for each individual core and adjusting the strain conversion coefficient in the transversal array of the gratings. Calibration also includes a measurement of the intrinsic twist of multicore fibres that has been introduced during the manufacturing process, whether by chance or intentionally. Overall, the maximum error of measuring curvature as well as the averaged relative error have been shown to become reduced by almost a factor of 2 in a test setup with curvature radii in a range between 40 mm and 70 mm. These results show the high importance of well adapted calibration procedures in shape sensing.

Acknowledgements

This work was performed within the framework of ITN-FINESSE, funded by the European Union's Horizon 2020 research and innovation programme under the Marie Sklodowska-Curie Action grant agreement n° 722509.

References

[1] M.J. Gander, W.N. MacPherson, R. McBride, J.D.C. Jones, L. Zhang, I. Bennion, P.M. Blanchard, J.G. Burnett, A.H. Greenaway, Bend measurement using Bragg gratings in multicore fibre, Electron. Lett. 36 (2000) 120–121. https://doi.org/10.1049/el:20000157..

[2] Ł. Szostkiewicz, M. A. Soto, Z.Yang, A. Dominguez-Lopez, I. Parola, K. Markiewicz, A. Pytel, A. Kołakowska, M. Napierała, T. Nasiłowski, L. Thevenaz, High-resolution distributed shape sensing using phase-sensitive optical time-domain reflectometry and multicore fibers, Opt. Express 27 (2019) 20763–20773. https://doi.org/10.1364/OE.27.020763.

[3] Z. Zhao, M. A. Soto, M. Tang, L. Thévenaz, Distributed shape sensing using Brillouin scattering in multi-core fibers, Opt. Express 24 (2016) 25211-25223. https://doi.org/10.1364/OE.24.025211.

[4] K. Bronnikov, A. Wolf, S. Yakushin, A. Dostovalov, O. Egorova, S. Zhuravlev, S. Semjonov, S. Wabnitz, S. Babin, Durable shape sensor based on FBG array inscribed in polyimide-coated multicore optical fiber, Opt. Express. 27 (2019) 38421. https://doi.org/10.1364/oe.380816.

[5] W. Zhuang, G. Sun, H. Li, X. Lou, M. Dong, :L. Zhu, FBG based shape sensing of a silicone octopus tentacle model for soft robotics, Optik 165 (2018) 7-15. https://doi.org/10.1016/j.ijleo.2018.03.087.

[6] K.R. Henken, J. Dankelman, J.J. Van Den Dobbelsteen, L.K. Cheng, M.S. Van Der Heiden, Error analysis of FBG-based shape sensors for medical needle tracking, IEEE/ASME Trans. Mechatronics. 19 (2014) 1523–1531. https://doi.org/10.1109/TMECH.2013.2287764.

[7] A.I. Gribaev, I. V. Pavlishin, A.M. Stam, R.F. Idrisov, S. V. Varzhel, K.A. Konnov, Laboratory setup for fiber Bragg gratings inscription based on Talbot interferometer, Opt. Quantum Electron. 48 (2016) 540. https://doi.org/10.1007/s11082-016-0816-3.

[8] J.P. Moore, M.D. Rogge, Shape sensing using multi-core fiber optic cable and parametric curve solutions, 20 (2012) 2967–2973. https://doi.org/10.1364/OE.20.002967.

[9] A. Ziolowicz, M. Szymanski, L. Szostkiewicz, T. Tenderenda, M. Napierala, M. Murawski, Z. Holdynski, L. Ostrowski, P. Mergo, K. Poturaj, M. Makara, M. Slowikowski, K. Pawlik, T. Stanczyk, K. Stepien, K. Wysokinski, M. Broczkowska, T. Nasilowski, Hole-assisted multicore optical fiber for next generation telecom transmission systems, Appl. Phys. Lett. 105 (2014) 081106. https://doi.org/10.1063/1.4894178.

[10] I. Floris, P.A. Calderón, S. Sales, J. M. Adam. Effects of core position uncertainty on optical shape sensor accuracy. Meas. J. Int. Meas. Confed. 139 (2019) 21-33. https://doi.org/10.1016/j.measurement.2019.03.031.